The foregoing boundary-value problem was solved with the aid of a digital computer. It was found that the arch buckles by sidesway (see Fig. 1), displaying bifurcations in the load-deflection curves. The calculated values of the critical load w and the critical vertical displacement v_c of the crown are presented in Fig. 2 for different subtending angles 2α. As seen from this figure, the larger the arch rise, the smaller is the intensity of the critical distributed load for given values of the initial radius a and flexural rigidity EI. Shallow arches have not been considered, as the inextensible theory yields accurate results for deep arches only.

Of some interest should be the comparison of the total critical weight $2\alpha aw$ with the critical concentrated downward load P at the crown of the arch. For example,

$$2\alpha aw = 24.4\, EI/a^2, \qquad P = 15.3\, EI/a^2 \quad \text{for } \alpha = 45°$$

$$2\alpha aw = 7.85\, EI/a^2, \qquad P = 5.86\, EI/a^2 \quad \text{for } \alpha = 90°$$

$$2\alpha aw = 1.17\, EI/a^2, \qquad P = 0.89\, EI/a^2 \quad \text{for } \alpha = 135°$$

where the critical values for P are taken from Refs. 9 and 11. (Remark: The critical values of $P = 6.17\ EI/a^2$ and $12.74\ EI/a^2$ for $\alpha = 90°$ and 53.1301°, respectively, as calculated by a finite element method in Refs. 14 and 15, do not agree well with our values of $5.86\ EI/a^2$ and $13.00\ EI/a^2$ which have been calculated by means of an exact theory.)

The foregoing comparison of buckling loads may be of some utility in the interpretation of test results for arches subjected to concentrated loads, since it is difficult to eliminate the effect of the dead weight of the arch tested.

References

[1] Timoshenko, S. P. and Gere, J. M., *Theory of Elastic Stability*, McGraw-Hill, New York, 1961.

[2] Rózsa, M., "Stability Analysis of Arches with Vertical Load," *Acta Technica*, Vol. 49, No. 3/4, 1964, Academia Scientifica Hungaricae, Budapest, Hungary, pp. 387–397.

[3] Langhaar, H. L., Boresi, A. P., and Carver, D. R., "Energy Theory of Buckling of Circular Elastic Rings and Arches," *Proceedings of Second U.S. National Congress of Applied Mechanics, ASME*, 1954, pp. 437–443.

[4] Lind, N. C., "Elastic Buckling of Symmetrical Arches," TR 3, 1962, Engineering Experiment Station, Univ. of Illinois.

[5] Nordgren, R. P., "On Finite Deflection of an Extensible Circular Ring Segment," *International Journal of Solids and Structures*, Vol. 2, No. 2, April 1966, pp. 223–233.

[6] Lo, C. F. and Conway, H. D., "The Elastic Stability of Curved Beams," *International Journal of Mechanical Sciences*, Vol. 9, No. 8, Aug. 1967, pp. 527–538.

[7] Conway, H. D. and Lo, C. F., "Further Studies on the Elastic Stability of Curved Beams," *International Journal of Mechanical Sciences*, Vol. 9, No. 10, Oct. 1967, pp. 707–718.

[8] Huddleston, J. V., "Finite Deflections and Snap-Through of High Circular Arches," *Journal of Applied Mechanics*, Vol. 35, No. 4, Dec. 1968, pp. 763–769.

[9] DaDeppo, D. A. and Schmidt, R., "Sidesway Buckling of Deep Circular Arches under a Concentrated Load," *Journal of Applied Mechanics*, Vol. 36, No. 2, June 1969, pp. 325–327.

[10] Schmidt, R. and DaDeppo, D. A., "Buckling of Deep Arches at Large Deflections," *AIAA Journal*, Vol. 7, No. 6, June 1969, pp. 1182–1183.

[11] DaDeppo, D. A. and Schmidt, R., "Nonlinear Analysis of Buckling and Postbuckling Behavior of Circular Arches," *Zeitschrift für angewandte Mathematik und Physik*, Vol. 20, No. 6, 1969, pp. 847–857.

[12] Wempner, G. A. and Kesti, N. E., "On the Buckling of Circular Arches and Rings," *Proceedings of the Fourth U.S. National Congress of Applied Mechanics, ASME*, Vol. 2, 1962, pp. 843–849.

[13] Schmidt, R. and DaDeppo, D. A., "Large Deflections of Eccentrically Loaded Arches," *Zeitschrift für angewandte Mathematik and Physik*, Vol. 21, No. 6, 1970, pp. 991–1004.

[14] Patrick, G. E., Jr., "Numerical Methods for the Nonlinear Analysis of an Elastic Arch," Rept. RS-TR-68-15, U.S. Army Missile Command, Redstone Arsenal, Ala., Dec. 1968.

[15] Wempner, G. A. and Patrick, G. E., Jr., "Finite Deflections, Buckling and Postbuckling of an Arch," *Proceedings of the Eleventh Midwestern Mechanics Conference*, Vol. 5, Iowa State Univ., Ames, Iowa, Aug. 1969, pp. 439–450.

Vibrations of Pressurized Orthotropic Shells

Clive L. Dym*

Carnegie-Mellon University, Pittsburgh, Pa.

Introduction

THE purpose of this short Note is to extend for the sake of completeness some previously published results on the vibration of pressurized orthotropic cylindrical membranes.[1] In that paper the effects of a) internal pressurization, b) the variation of elastic constants, and c) the deletion of the inplane inertia, upon the free and forced vibrations of membrane shells was examined. The present analysis will display the effects of these physically important parameters upon the free vibrations of shells where the bending terms are included.

Analysis

The formulation is based on the nonlinear strain-displacement relations used in the theory of shallow shells. With u^*, v^*, w^* being the dimensional displacements they take the form

$$\begin{aligned} \epsilon_{xx} &= \partial u^*/\partial x + \tfrac{1}{2}(\partial w^*/\partial x)^2 - z\partial^2 w^*/\partial x^2 \\ \epsilon_{yy} &= \partial v^*/\partial y - w^*/R + \tfrac{1}{2}(\partial w^*/\partial y)^2 - z\partial^2 w^*/\partial y^2 \\ \gamma_{xy} &= \partial u^*/\partial y + \partial v^*/\partial x + (\partial w^*/\partial x)\partial w^*/\partial y - 2z\partial^2 w^*/\partial x\partial y \end{aligned} \tag{1}$$

These kinematic equations are used in conjunction with the linear orthotropic relations for a conservative material in a state of plane stress

$$\tau_{xx} = C_{11}\epsilon_{xx} + C_{12}\epsilon_{yy}$$
$$\tau_{yy} = C_{12}\epsilon_{xx} + C_{22}\epsilon_{yy}, \ \tau_{xy} = G_{12}\gamma_{xy} \tag{2}$$

and Hamilton's principle to derive the following set of equilibrium equations:

$$\frac{\partial N_{xx}}{\partial x} + \frac{\partial N_{xy}}{\partial y} = \frac{\partial^2 u^*}{\partial t^2}, \quad \frac{\partial N_{xy}}{\partial x} + \frac{\partial N_{yy}}{\partial y} = \frac{\partial^2 v^*}{\partial t^2} \tag{3a}$$

$$\frac{\partial^2 M_{xx}}{\partial x^2} + 2\frac{\partial^2 M_{xy}}{\partial x\partial y} + \frac{\partial^2 M_{yy}}{\partial y^2} + \frac{\partial}{\partial x}\left(N_{xx}\frac{\partial w^*}{\partial x} + N_{xy}\frac{\partial w^*}{\partial y}\right) + \frac{\partial}{\partial y}\left(N_{xy}\frac{\partial w^*}{\partial x} + N_{yy}\frac{\partial w^*}{\partial y}\right) + \frac{1}{R}N_{yy} = \frac{\partial^2 w^*}{\partial t^2} \tag{3b}$$

Here the N_{ij} and M_{ij} are the usual stress and moment result-

Received January 4, 1971; revision received February 8, 1971. The author is extremely grateful to J. F. Oyler of the Dravo Corporation, Pittsburgh, Pa., for his assistance in assembling the numerical results.

* Associate Professor of Civil Engineering. Member AIAA.

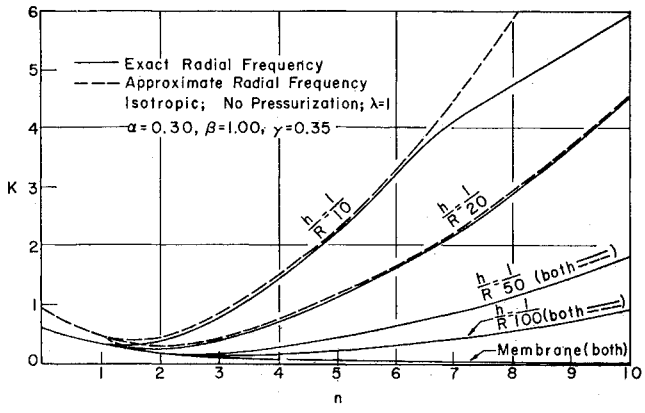

Fig. 1 Radial frequency factor vs circumferential wave number.

ants, and the reduction to the membrane equations given in Ref. 1 are accomplished by setting the M_{ij} equal to zero, and writing the N_{ij} as t_{ij}.

Equations (3) are then linearized about an internal pressure state given as $N_{xx}{}^0 = \tau_{xx}{}^0 h$, $N_{yy}{}^0 = \tau_{yy}{}^0 h$, and this linearized set can be expressed in terms of the perturbation displacements u, v and w as follows:

$$C_{11}\frac{\partial^2 u}{\partial x^2} + G_{12}\frac{\partial^2 u}{\partial y^2} + (C_{12}+G_{12})\frac{\partial^2 v}{\partial x \partial y} - C_{12}\frac{1}{R}\frac{\partial w}{\partial x} = \rho\frac{\partial^2 u}{\partial t^2} \quad (4a)$$

$$(C_{12}+G_{12})\frac{\partial^2 u}{\partial x\partial y} + G_{12}\frac{\partial^2 v}{\partial x^2} + C_{22}\frac{\partial^2 v}{\partial y^2} - C_{22}\frac{1}{R}\frac{\partial w}{\partial y} = \rho\frac{\partial^2 v}{\partial t^2} - \frac{1}{12}\left(\frac{h}{R}\right)^2\left[C_{11}\frac{\partial^4 w}{\partial x^4} + (2C_{12}+4G_{12})\frac{\partial^4 w}{\partial x^2\partial y^2} + C_{22}\frac{\partial^4 w}{\partial y^4}\right] + C_{12}\frac{1}{R}\frac{\partial u}{\partial x} + C_{22}\frac{1}{R}\left(\frac{\partial v}{\partial y} - \frac{w}{R}\right) + \tau_{xx}{}^0\frac{\partial^2 w}{\partial x^2} + \tau_{yy}{}^0\frac{\partial^2 w}{\partial y^2} = \rho\frac{\partial^2 w}{\partial t^2} \quad (4b)$$

Note the appearance of the thickness-to-radius ratio in the radial equilibrium equation that arises from the inclusion of the bending terms.

To examine the free vibration natural frequencies of the pressurized shell, a Rayleigh-type solution is postulated, that is

$$u(x,y,t) = A_{mn}\cos(m\pi x/L)\cos(ny/R)\cos\omega t$$
$$v(x,y,t) = R_{mn}\sin(m\pi x/L)\sin(ny/R)\sin\omega t \quad (5)$$
$$w(x,y,t) = C_{mn}\sin(m\pi x/L)\cos(ny/R)\cos\omega t$$

where ω is the natural frequency expressed in radians-per-second. This solution satisfies the boundary conditions (at $x = 0,L$) of a simply supported shell, i.e.,

$$N_{xx} = M_{xx} = v = w = 0 \qquad \text{at } x = 0,\ L \quad (6)$$

(Of course, in Eq. (6), all the quantities are perturbation quantities.)

Substitution of the solutions (5) into the differential Eqs. (4) yields a system of three linear algebraic equations for the coefficients A_{mn}, B_{mn}, C_{mn}. Written in matrix form they are

$$\begin{bmatrix} (K^2-\lambda^2-\gamma n^2) & (\alpha+\gamma)n\lambda & -\alpha\lambda \\ (\alpha+\gamma)n\lambda & (K^2+\gamma\lambda^2-\beta n^2) & \beta n \\ -\alpha\lambda & \beta n & (K^2-\bar{H}-t_{x0}\lambda^2-t_{y0}n^2-\beta) \end{bmatrix} \times \begin{Bmatrix} A_{mn} \\ B_{mn} \\ C_{mn} \end{Bmatrix} = 0 \quad (7)$$

To write Eq. (7) in this compact form, the following quantities have been introduced:

$$K = \text{frequency factor} = (\rho/C_{11})^{1/2}R\omega$$
$$\lambda = \text{axial wave length factor} = m\pi R/L$$
$$\alpha = C_{12}/C_{11}, \quad \beta = C_{22}/C_{11}, \quad \gamma = G_{12}/C_{11} \quad (8)$$
$$\bar{H} = \tfrac{1}{12}(h/R)^2[\lambda^4 + (2\alpha+4\gamma)\lambda^2 n^2 + \beta n^4]$$
$$t_{x0} = \tau_{xx}{}^0/C_{11}, \quad t_{y0} = \tau_{yy}{}^0/C_{11}$$

A nontrivial solution to the system Eq. (7) can exist only if the determinant of the coefficient vanishes. This yields a cubic equation in the square of the frequency factor K. Thus for each mode (aach pair λ, n), three frequencies are found, the lowest of which corresponds to motion that is predominantly radial.

It is possible to obtain a much simpler solution for this low (radial) frequency by deleting the inplane inertia terms in Eqs. (4). This corresponds to deleting the K^2 terms in the first two of Eqs. (7), which yields after a straight forward calculation the following explicit expression for the radial frequency factor:

$$K_{\text{rad}}{}^2 = t_{x0}\lambda^2 + t_{y0}n^2 + (\beta-\alpha^2)\lambda^4/\{\lambda^4 + [(\beta-\alpha^2)/\gamma - 2\alpha]\lambda^2 n^2 + \beta n^4\} + \tfrac{1}{12}(h/R)^2[\lambda^4 + (2\alpha+4\gamma)\lambda^2 n^2 + \beta n^4] \quad (9)$$

If the ratio h/R is allowed to vanish, the resulting expression will be that of the radial frequency of the membrane shell [Eq. (24) of Ref. 1]. For the isotropic shell [$\alpha = \nu$, $\beta = 1$, $\gamma = (1-\nu)/2$], the result Eq. (9) is further simplified:

$$K_{\text{rad}}{}^2 = \frac{\tau_{xx}{}^0}{E}\lambda^2 + \frac{\tau_{yy}{}^0}{E}n^2 + \frac{(1-\nu^2)\lambda^4}{(\lambda^2+n^2)^2} + \frac{1}{12}\left(\frac{h}{R}\right)^2(\lambda^2+n^2)^2 \quad (10)$$

Before proceeding to the numerical results it is of interest to point out that Eqs. (9) and (10) may be used for the explicit calculation of buckling loads, achieving precisely the order of accuracy obtainable from the well-known linearized eighth-order Donnell equation.† This may be done on the basis of

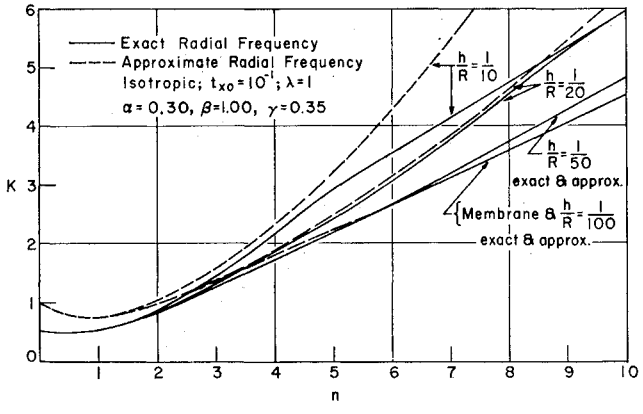

Fig. 2 Radial frequency factor vs circumferential wave number.

† Of course this is hardly surprising since a linearized shallow shell theory without in-plane inertia was used to obtain Eq. (9).

the "vibration" approach to stability, where one seeks those values of compressive loads for which the frequency vanishes.[2] Thus if τ_{xx}^0 and τ_{yy}^0 (or t_{x0} and t_{y0}) are taken as positive in compression, one obtains from Eq. (9) the result that

$$\left(\frac{\tau_{xx}^0}{C_{11}}\right)_{\text{crit}} \lambda^2 + \left(\frac{\tau_{yy}^0}{C_{11}}\right)_{\text{crit}} n^2 = \frac{(\beta - \alpha^2)\lambda^4}{\lambda^4 + [(\beta - \alpha^2)/\gamma - 2\alpha]\lambda^2 n^2 + \beta n^4} + \frac{1}{12}\left(\frac{h}{R}\right)^2 [\lambda^4 + (2\alpha + 4\gamma)\lambda^2 n^2 + \beta n^4] \quad (11)$$

From Eq. (11) the critical loads for simple axial compression ($\tau_{yy}^0 = 0$), simple radial pressure ($\tau_{xx}^0 = 0, \tau_{yy}^0 = pR/h$) and hydrostatic pressure ($\tau_{xx}^0 = 1/2\tau_{yy}^0 = pR/2h$) are obtained by appropriate minimization with respect to λ and n. An interesting algorithm for accomplishing this task has recently been given by Pappas and Amba-Rao.[3]

Results

The results obtained by evaluating the lowest eigenvalue of the matrix Eq. (7) and the approximate radial frequency of Eq. (9) are displayed in Figs. 1–2. One thing that is clear immediately is the very good agreement between these two solutions, excepting only the case of a thick shell ($h/R = 1/10$) where the validity of a thin shell theory may be questionable, and in the range of $n = 2$ where the Donnell-type shell theories may not be entirely accurate.

Comparison of Figs. 1 and 2 indicates the effects of internal pressurization. One result is that the pressures drive up the frequency for a given geometry and wave number. This driving effect appears to be larger, for a given internal pressure, on the thinner shells. Another result of the pressurization is that the membrane frequencies no longer vanish as $n \to \infty$.

Similar calculations were carried out with a sharp reduction in the circumferential stiffness, in fact a drop of 80% in that stiffness. The qualitative results just indicated hold for the orthotropic shell also, except that for large wave numbers the pressurization effect makes the variation of the elastic constants negligible. In the absence of pressurization, or for small wave numbers in the presence of pressurization, the drop in the circumferential stiffness yields a sizable decrease in the frequencies of free vibration.

In other results not displayed for the sake of brevity, it is also found that the frequencies of the inplane modes of vibration are virtually insensitive to changes in the thickness-to-radius ratio of the shell for reasonably thin shells ($h/R \leq 1/20$].

Conclusions

The principal conclusions are as follows: 1) the deletion of the inplane inertia terms allows in most cases of bending of orthotropic shells a very good approximation of the "radial" frequency; 2) the change of circumferential stiffness yields sizable changes in the free vibration frequency of the radial mode; and 3) the introduction of pressurization can increase the shell's radial frequency substantially, and can eliminate entirely changes due to a decrease in the circumferential stiffness.

References

[1] Dym, C. L., "Vibrations of Pressurized Orthotropic Cylindrical Membranes," *AIAA Journal*, Vol. 8, No. 4, April 1970, pp. 693–699.

[2] Ziegler, H., *Principles of Structural Stability*, Blaisdell, Waltham, Mass., 1968, pp. 12–14.

[3] Pappas, M., and C. L. Amba-Rao, "A Discrete Search Procedure for the Minimization of Stiffened Cylindrical Shell Stability Equations," *AIAA Journal*, Vol. 8, No. 11, Nov. 1970, pp. 2093–2094.

Effect of Angle of Attack on Boundary-Layer Transition at Mach 21

MICHAEL C. FISCHER* AND DAVID H. RUDY*
NASA Langley Research Center, Hampton, Va.

Nomenclature

M	=	Mach number
$\dot{q}$	=	convective heat-transfer rate, w/m^2
R	=	Reynolds number
r_n	=	nose radius, cm
$T_{t,\infty}$	=	total temperature, °K
T_w	=	wall temperature, °K
X	=	distance along cone surface from tip, cm
θ_c	=	cone half-angle, deg

Subscripts

e	=	cone boundary-layer edge conditions at $\alpha = 0°$
E,tr	=	end of transition
S,tr	=	start of transition
∞	=	freestream conditions

FOR Mach numbers less than 11, the investigations of Refs. 1–5 indicate that angle of attack promotes sharp cone boundary-layer transition on the leeward ray while retarding transition on the windward ray. This behavior is usually attributed to the instability of the crossflow from the windward to the leeward side. However, the investigation of Ref. 6 with $M_\infty \approx 20$ and $M_e(\alpha = 0°) \approx 16$ indicated a trend opposite to this. That is, transition was retarded on the leeward ray and promoted on the windward ray. This conflicting behavior was attributed to the large local Mach number changes caused by angle of attack and the subsequent effect of this local Mach number change on transition. The present investigation is intended to reassess the results of Ref. 6 and extend the transition data over a wider angle-of-attack range utilizing alternate instrumentation. Testing occurred in the same facility as for the previous investigation[6] and employed a cone of identical external geometry.

The model used in the present investigation was a 152.4 cm long, 2.87° half-angle smooth cone, fabricated from 347 stainless steel and instrumented with thermocouples and pressure orifices. Skin thickness at the thermocouple location was 0.015 cm and nose radius 0.010 cm. The data were obtained in the Langley 22-in. Mach 20 helium tunnel which has an axisymmetric contoured nozzle. Angle of attack was in the range $\alpha = 0°$–3° with the freestream Reynolds number maintained at about 0.47×10^6/cm. All tests were conducted in unheated flow ($T_{t,\infty} \approx 300$°K) with $T_w/T_{t,\infty} \approx 1.0$ and a freestream Mach number of 21.5.

Typical heat-transfer distributions on the cone surface are presented in Fig. 1 for $\alpha = 0°$ and $\alpha = 1°$. Since these tests were conducted at $T_w/T_{t,\infty} \approx 1.0$, the heat flux was from the model to the flow ($-\dot{q}$). The boundary-layer transition location was taken as the location where the heat-transfer data first departed from the laminar level. The results of the present transition measurements, shown in Fig. 2, along with the results of Ref. 6, indicate that transition generally moves forward on the leeward ray with little movement on the windward ray, except for $\alpha = 0°$–1° where an apparent reversal takes place on both rays. This result is in direct conflict with the findings of Ref. 6. Since both investigations were conducted in the same facility and both models had the same external geometry with nearly identical nose radii the discrepancy in results is attributed to the different methods of transition detection. Additional tests were conducted using a 0.0025-cm nose radius tip with no measurable change occurring

Received January 25, 1971.

* Aerospace Engineer, Viscous Flow Section, Hypersonic Vehicles Division.